

Enhancing the performance of Cu catalysts for the Reverse Water Gas Shift Reaction using N-doped CNT-ZnO composite as support

Ana Rita Querido,^{a,b} Liliana P. L. Gonçalves,^{a,b,c} Yury V. Kolen'ko^c, M. Fernando R. Pereira^{a,b}, O. Salomé G. P. Soares,^{a,b,*}

¹ LSRE-LCM - Laboratory of Separation and Reaction Engineering, Laboratory of Catalysis and Materials, Faculty of Engineering, University of Porto, Rua Dr. Roberto Frias, 4200-465, Porto, Portugal

² ALiCE - Associate Laboratory in Chemical Engineering, Faculty of Engineering, University of Porto, Rua Dr. Roberto Frias, 4200-465, Porto, Portugal

³ International Iberian Nanotechnology Laboratory, Avenida Mestre José Veiga s/n, 4715-330 Braga, Portugal

*Corresponding author: salome.soares@fe.up.pt

Experimental Methods

Characterization Methods

N₂ adsorption-desorption isotherms at -196 °C were used to determine the textural properties of the samples, including specific surface area (S_{BET}) and pore volume of the samples (V_p). The analysis was performed in a NOVA 4200e Surface Area & Pore Size Analyzer where the samples ($m \approx 100$ mg) were degassed at 170 °C for 3 h before the analysis. The model employed to determine S_{BET} was the BET equation (Brunauer, Emmet and Teller), the most commonly used model to determine porous materials' surface areas, applicable to relative pressures with values between 0.05 and 0.30.

The elemental analysis procedure was performed on a vario MICRO cube and a rapid OXY cube analysers from Elemental. Each sample suffered combustion at 1050 °C, determining each element by the mean of 3 independent measurements, using a per-day calibration with a standard compound.

Temperature programmed desorption (TPD) was used to analyse the surface groups on the oxidized supports. Analysis was carried out on an AMI-300 catalyst characterization apparatus by Altamira Instruments, equipped with a thermal conductivity detector (TCD), a mass spectrometer (MS), high precision mass flow controllers and a furnace with air cooling. Approximately 100 mg of a sample was placed in a U-shaped quartz reactor which was then placed in the equipment's furnace and the temperature was increased, under He flow rate of 25 cm³ min⁻¹, until 1050 °C. CO and CO₂ released by the sample were analyzed by MS.

The optimal reduction temperature of the various catalysts was determined by H₂ – Temperature Programmed Reduction (H₂-TPR), in an AMI-200 and AMI-300 equipment's (Altamira Instruments), both equipped with a thermal conductivity detector (TCD). Analysis was carried out on ca. 100 mg of each

sample in a U-shaped quartz reactor. As a first step, the tube was flushed under a $25 \text{ cm}^3 \text{ min}^{-1}$ flow rate of Ar, followed by the heating of the samples until $1000 \text{ }^\circ\text{C}$, with a heating rate of $10 \text{ }^\circ\text{C min}^{-1}$, under a flow of diluted H_2 (5% H_2/Ar).

Powder X-ray diffraction analysis (XRD) was carried out on a PANalytical X'Pert PRO diffractometer with Ni filtered $\text{Cu K}\alpha$ radiation and PIXcel detector. Samples were grounded into a fine powder, placed in a sample holder, and were analyzed using a Bragg Brentano configuration in a 2θ range (20° to 80°) with a step size of 0.01° (200 s per step). The gathered data was analyzed using the PANalytical High Score software.

X-ray photoelectron spectroscopy (XPS) was performed in a ESCALAB 250Xi (Thermo Scientific) using a monochromated microfocused $\text{Al K}\alpha$ X-ray source. Powdered samples were pressed into carbon tape, which was directly attached to the sample holder. Charge neutralization was accomplished by an "in lens" flood gun. XPS analysis was performed using the Avantage software (Thermo Fisher Scientific), in which the peaks were fitted with a Gaussian-Lorentzian function. Binding energies were calibrated relative to the C 1s peak for aliphatic and aromatic carbon at 284.8 eV .

Transmission electron microscopy analysis (TEM) observations were conducted using a JEOL 2100 electron microscope operated at 200 kV . The samples were prepared by dispersing powder samples in ethanol and dropping the dispersion onto a carbon coated copper grid.

Scanning Transmission electron microscopy analysis (STEM) was carried out on a FEI Titan ChemiSTEM microscope operating at 200 kV . Energy-dispersive X-ray spectroscopy in STEM mode (STEM-EDX) was performed using the same equipment. The samples were prepared similarly as in TEM.

Additional Catalytic Experiments

The catalytic experiments performed, mainly consisted in evaluating the effect of the support on Cu-based catalysts for the RWGS reaction.

Catalytic testing began with a preliminary test that consisted in evaluating the performance of Cu-based catalysts, with a fixed loading of 15% wt, supported on pristine AC and CNTs (Figure S1).

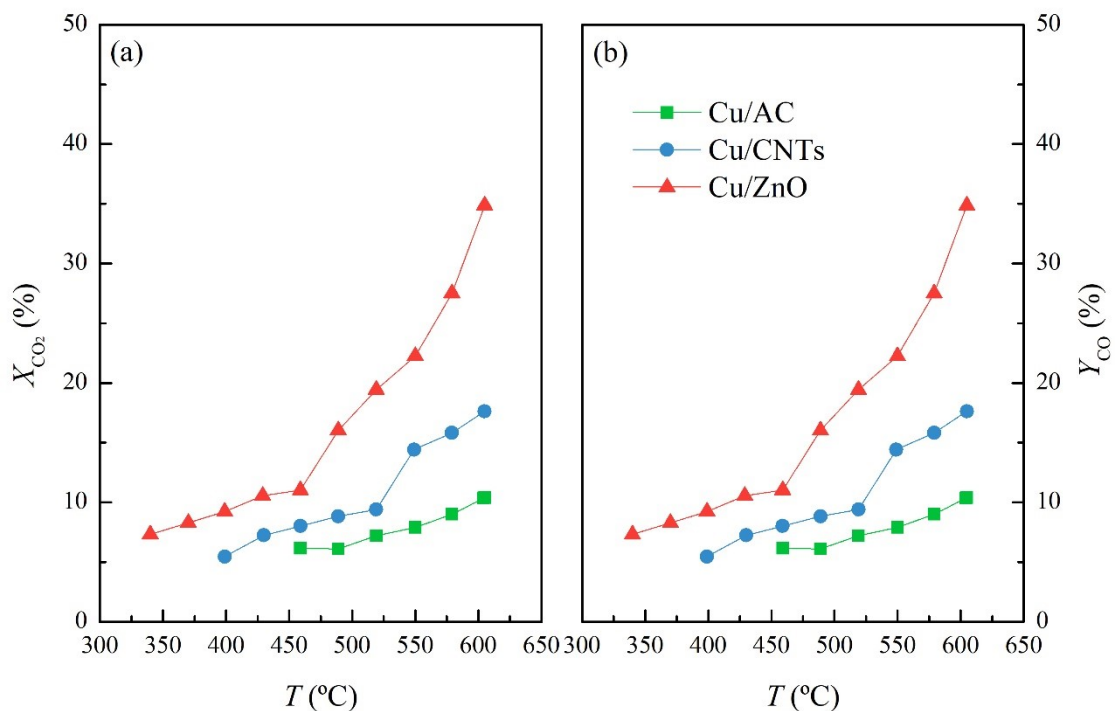


Figure S1. Comparison of the catalytic performance, in terms of X_{CO_2} (a) and Y_{CO} (b), at different temperatures, for Cu supported on pristine AC and CNT, as well as for the reference catalyst, Cu supported on ZnO. Reaction conditions: $P = 1$ bar; $GHSV = 60\,000\text{ cm}^3\text{ g}^{-1}\text{ h}^{-1}$; $CO_2:H_2 (V:V) = 1:4$.

As expected, the performance from all catalysts achieves its higher results at the highest temperature, 600 °C, due to the endothermic nature of the RWGS reaction. The catalytic performance of the reference catalyst²², Cu/ZnO, is better than the catalysts supported on pristine carbon materials, with $X_{CO_2} = 34.9\%$ at a temperature of 600 °C. Comparing the catalytic performance of the catalysts supported on pristine carbon materials, the catalysts supported on CNTs demonstrated better catalytic results, with $X_{CO_2} = 17.6\%$ at a temperature of 600 °C, while the catalysts supported on AC achieved a $X_{CO_2} = 10.4\%$ at a temperature of 600 °C. All the referred catalysts demonstrated 100% selectivity to CO.

Additional Characterization

N₂ Physisorption at -196 °C

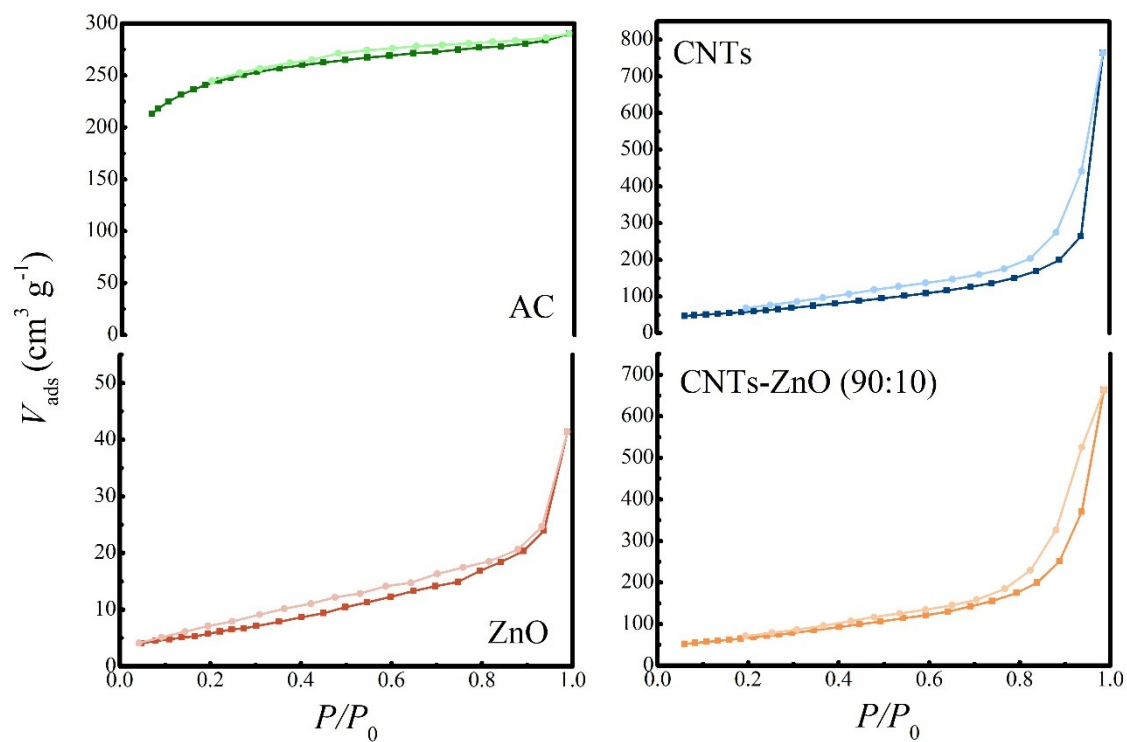


Figure S2. N₂ adsorption-desorption isotherms at -196 °C measured for AC, CNTs, AC-ZnO (90:10), CNTs-ZnO (90:10), and ZnO.

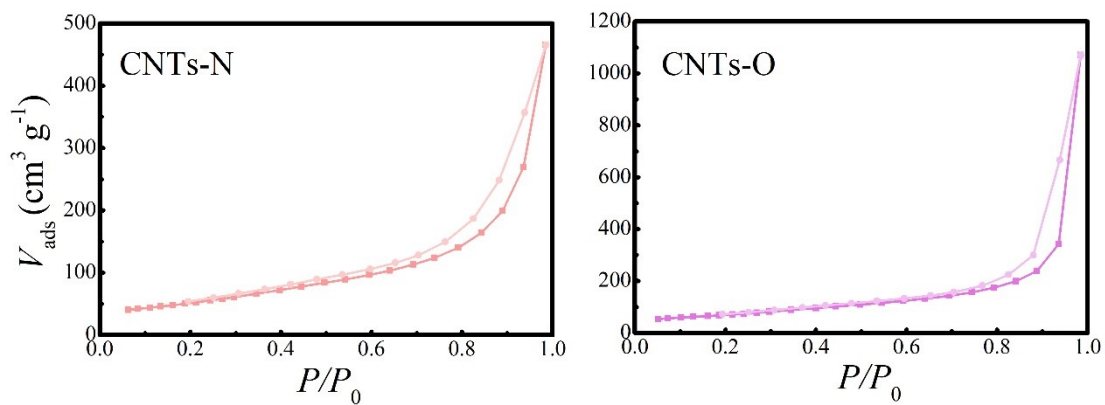


Figure S3. N₂ adsorption-desorption isotherms at -196 °C measured for CNTs-N and CNTs-O.

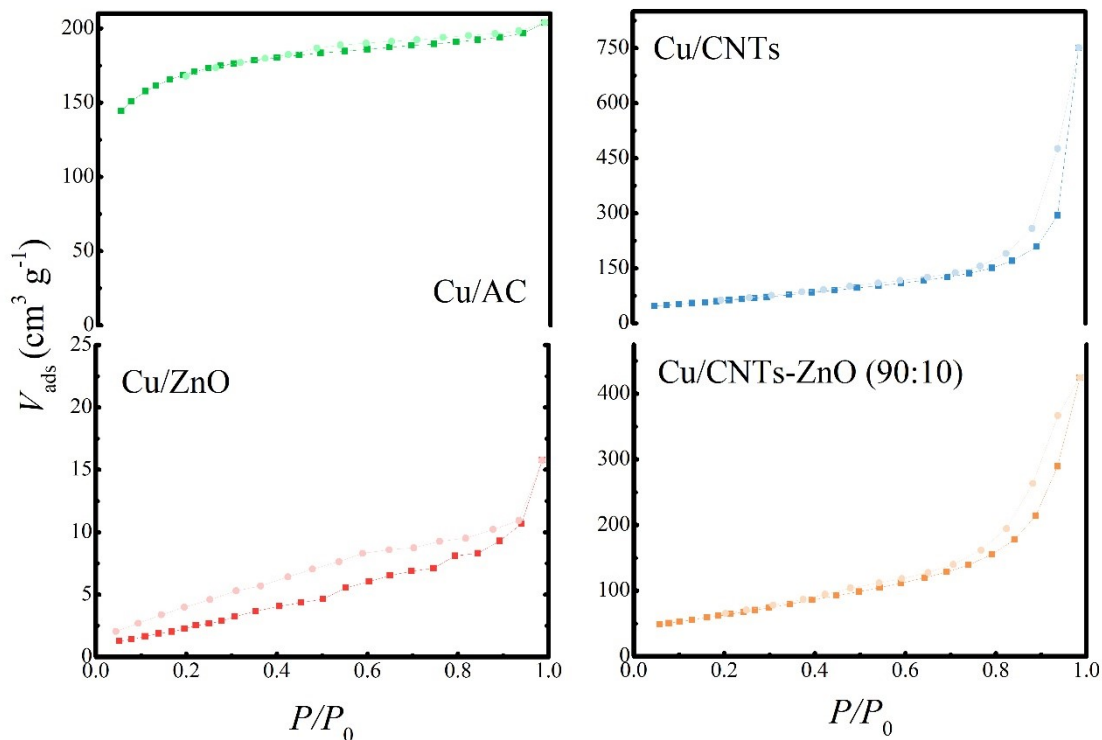


Figure S4. N₂ adsorption–desorption isotherms at $-196\text{ }^{\circ}\text{C}$ measured for Cu/AC, Cu/CNTs, Cu/ZnO, and Cu/CNTs-ZnO (90:10).

Table S1. Textural properties of the supporting materials and catalysts.

| Sample | S_{BET} [$\text{m}^2\text{ g}^{-1}$] | $V_{P, P/P_0=0.95}$ [$\text{cm}^{-3}\text{ g}^{-1}$] | V_{Micro} [$\text{cm}^{-3}\text{ g}^{-1}$] |
|-----------------------|---|---|---|
| AC | 792 | 0.438 | 0.347 |
| CNTs | 209 | 0.409 | 0 |
| CNTs-N | 191 | 0.417 | 0 |
| CNTs-O | 254 | 0.531 | 0 |
| CNTs-ZnO (90:10) | 245 | 0.573 | 0 |
| ZnO | 23.5 | 0.037 | 0 |
| Cu/AC | 546 | 0.304 | 0.245 |
| Cu/CNTs | 223 | 0.455 | 0 |
| Cu/CNTs-ZnO (90:10) | 231 | 0.448 | 0 |
| Cu/CNTs-N-ZnO (90:10) | 143 | 0.284 | 0 |
| Cu/ZnO | 11.2 | 0.017 | 0 |

Pristine AC presents a type I+II isotherm and a type H4 hysteresis, according to the IUPAC classification²³. The mainly microporous nature of AC materials is confirmed by the significant

increase of N_2 adsorption at the lower levels of P/P_0 . Nevertheless, it is expected that these materials also possess slit-like mesopores, demonstrated by the small increase of N_2 adsorption at higher levels of P/P_0 . According to IUPAC, the hysteresis seen in the AC materials isotherms is typical of materials with small slit-like pores and micro-mesoporous carbons ²³.

Elemental Analysis

Table S2. Elemental composition of the pristine and functionalized carbon materials.

| <i>Sample</i> | <i>N</i> (%) | <i>C</i> (%) | <i>H</i> (%) | <i>O</i> (%) |
|---------------|-----------------|-----------------|-----------------|-----------------|
| <i>AC</i> | 0.06 | 84.7 | 0.85 | 7.51 |
| <i>CNT</i> | 0.02 | 91.0 | 0.31 | 3.82 |
| <i>CNT-N</i> | 7.53 | 83.5 | 0.58 | 5.95 |
| <i>CNT-O</i> | 0.1 | 92.1 | 0.42 | 6.8 |

Temperature Programmed Desorption

Table S3. CO and CO₂ released during TPD analysis on AC, CNTs and CNTs-O.

| <i>Sample</i> | <i>[CO]</i> [$\mu\text{mol g}^{-1}$] | <i>[CO₂]</i> [$\mu\text{mol g}^{-1}$] |
|---------------|---|---|
| <i>AC</i> | 720 | 270 |
| <i>CNT</i> | 310 | 160 |
| <i>CNT-O</i> | 1584 | 900 |

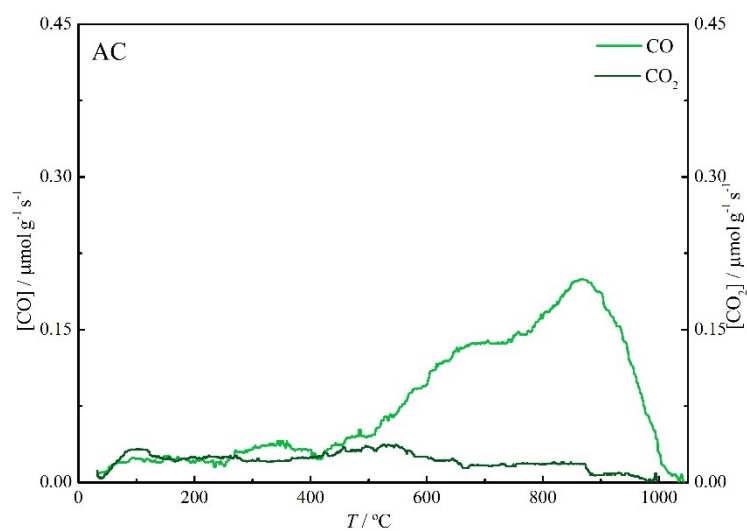


Figure S5. TPD profiles for pristine AC.

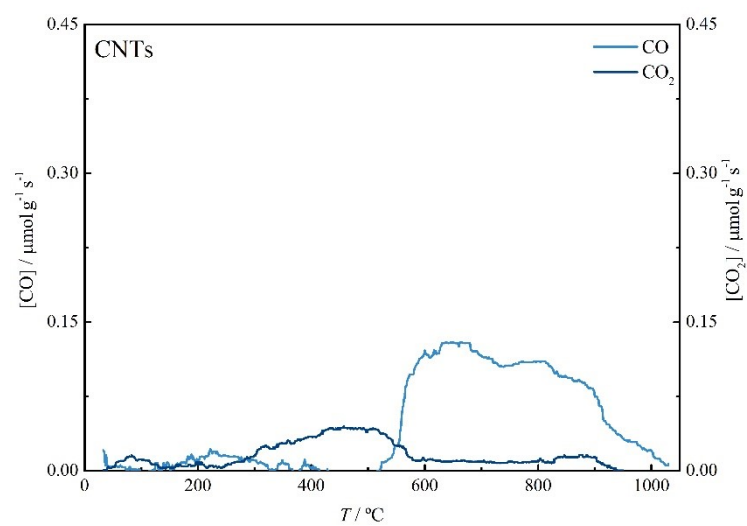


Figure S6. TPD profiles for pristine CNTs.

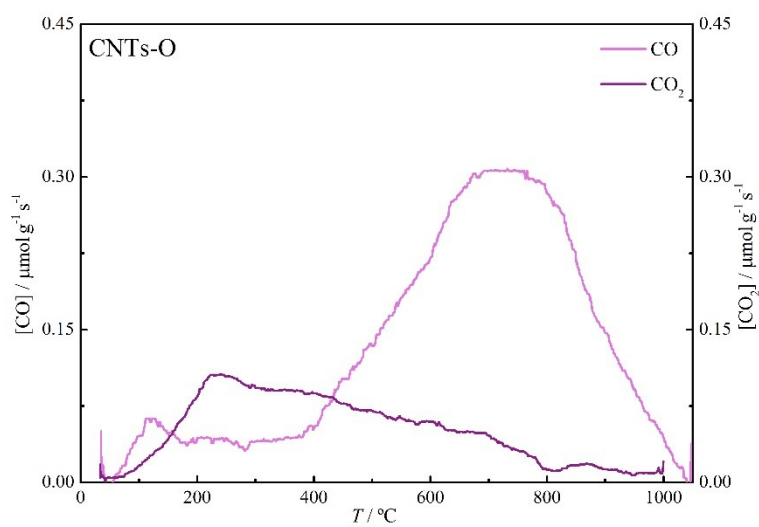


Figure S7. TPD profiles for CNTs-O.

Pristine AC (Figure S5) emits a small amount of CO₂ (Table S3); therefore, it was concluded that AC materials present small quantities of carboxylic acids, anhydrides and lactone groups in their surface. Pristine AC also releases a small amount of CO (Table S3), in a similar temperature range, hence it was concluded that pristine AC contains anhydrides, phenol, carbonyl, ether and quinone groups in its surface. Nevertheless, it should be noted that pristine AC releases a bigger amount of CO₂ and CO than pristine CNTs, thus it also presents a greater amount of the mentioned O-groups in its surface^{25,26}.

H₂ – Temperature Programmed Reduction (H₂-TPR)

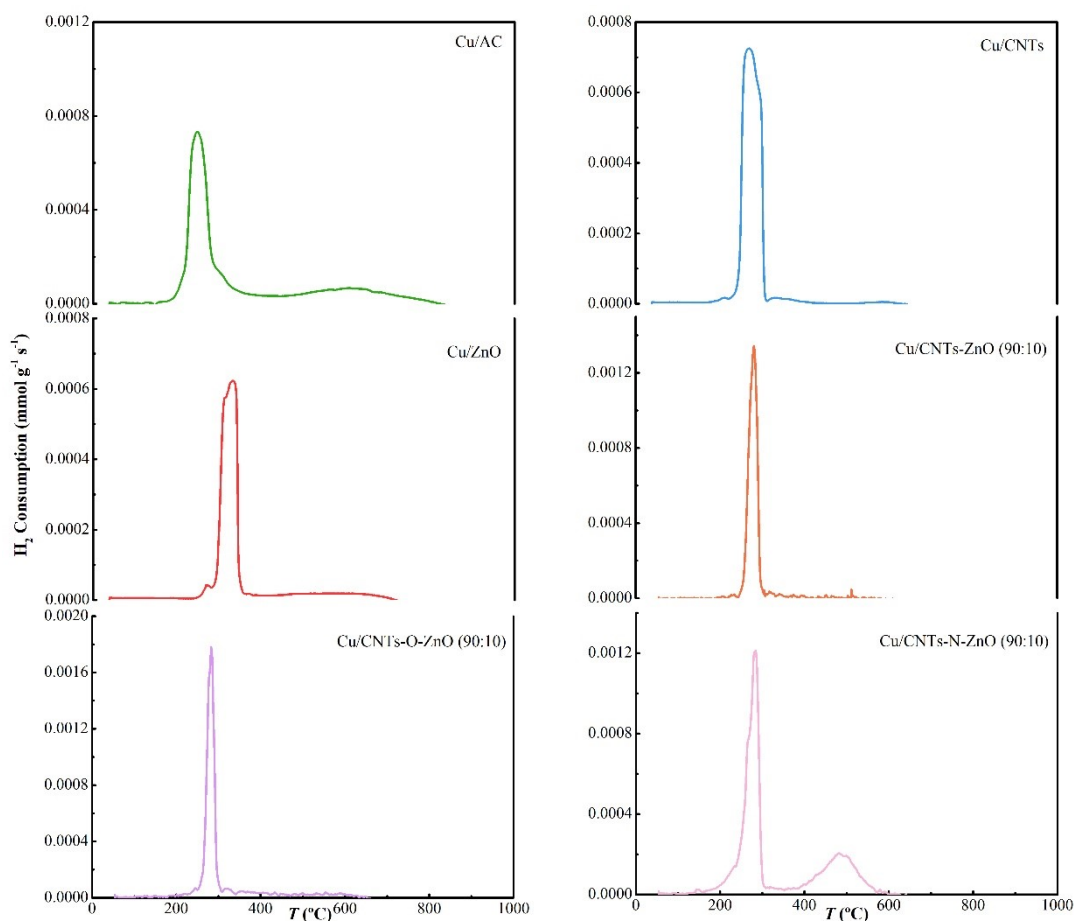


Figure S8. H₂-TPR profiles of Cu/AC, Cu/CNTs, Cu/ZnO, Cu/CNTs-ZnO (90:10), Cu/CNTs-O-ZnO (90:10), and Cu/CNTs-N-ZnO (90:10).

Comparing the catalysts supported on pristine AC, CNTs, and ZnO with the same amount of Cu (15% wt) (Figure S8), it becomes clearer that AC, as a support, increases the reducibility of the catalyst, with its H₂ consumption beginning early on, after 200 °C. Therefore, the supports can be arranged by their reducibility as: AC > CNTs > ZnO. The AC supported catalyst, presents two peaks for two different types of Cu species; a peak at higher temperatures that correspond to species

that present a stronger interaction with the support, and a peak at lower temperatures corresponding to species that present a weaker interaction with the support. Although Cu/AC presents two peaks while Cu/CNTs presents only one, the peak with the larger area for Cu/AC occurs at a lower temperature than Cu/CNT. It was then concluded that, Cu/AC presents a weaker metal-support interaction than Cu/CNTs thus, its particle size may be larger. For the catalysts supported on pristine AC the reduction temperature was determined as 200 °C.

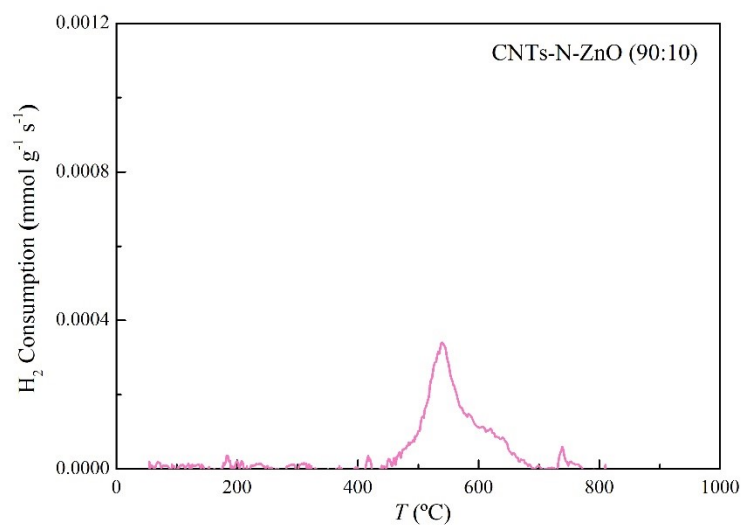


Figure S9. H₂-TPR profile of CNTs-N-ZnO (90:10).

Powder X-ray diffraction (XRD)

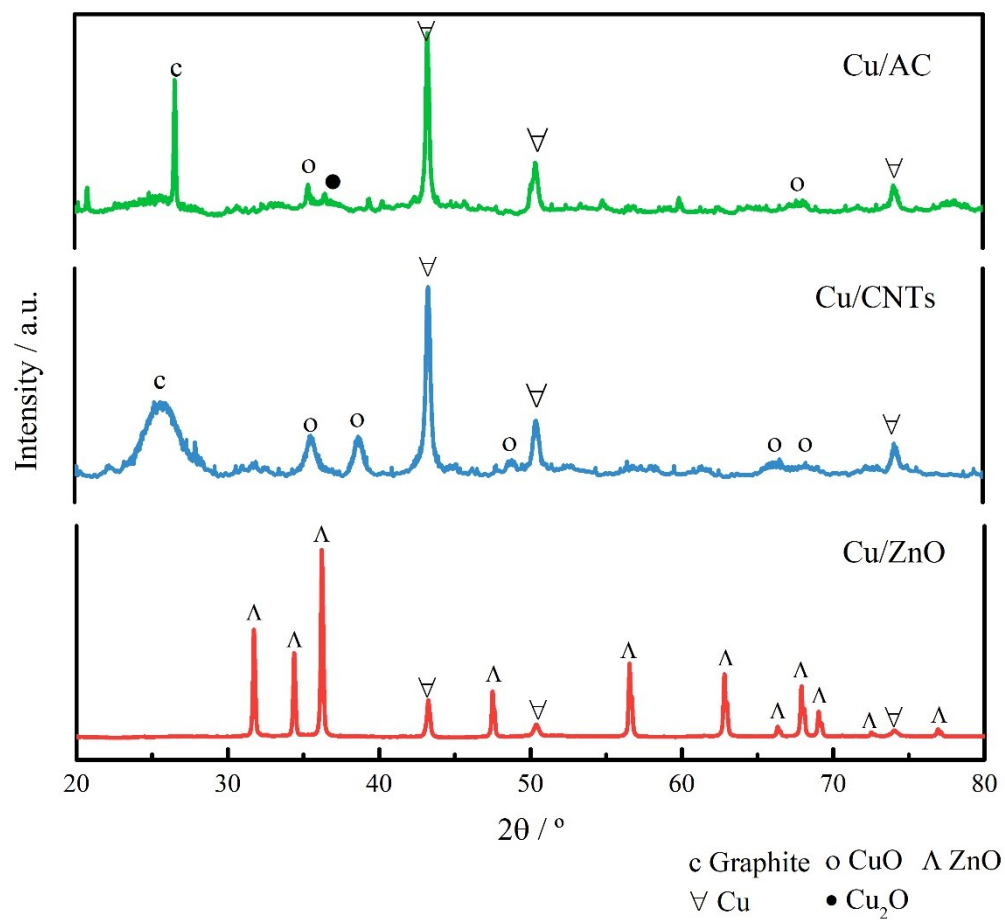


Figure S10. XRD patterns of the performing catalysts: Cu/AC, Cu/CNTs, and Cu/ZnO.

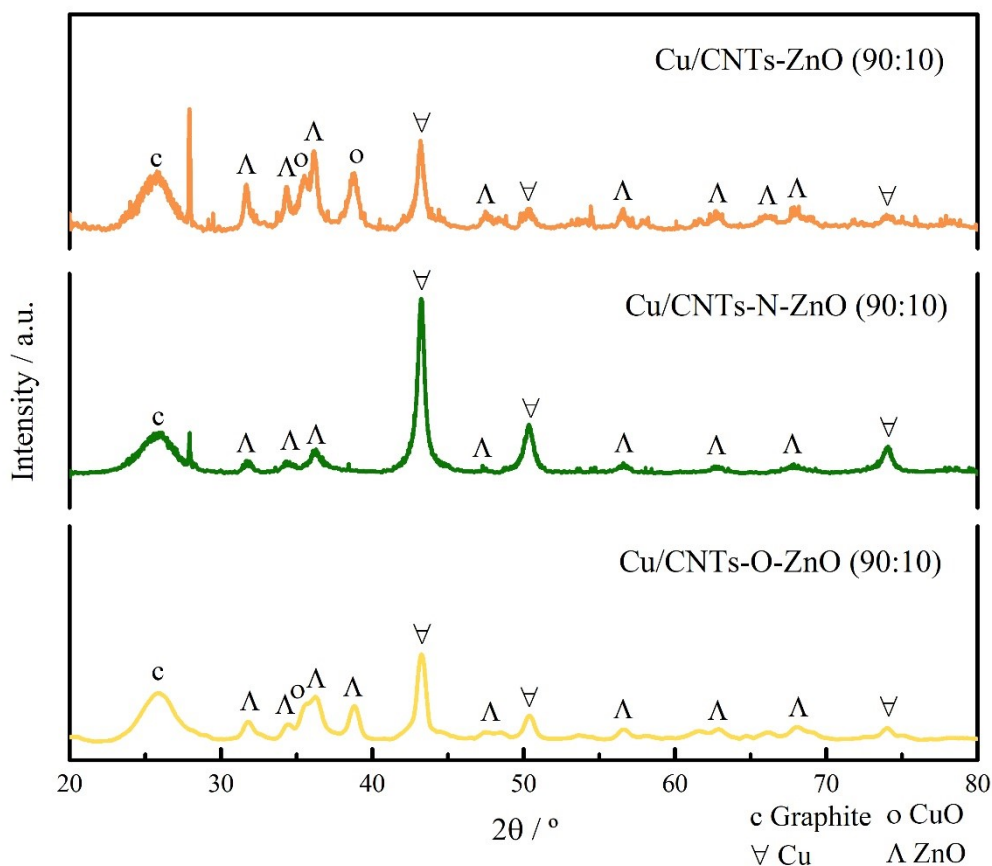


Figure S11. XRD patterns of the catalysts: Cu/CNTs-N-ZnO (90:10) and Cu/CNTs-O-ZnO (90:10).

For the Cu/AC catalyst, peaks were detected at $2\theta = 43.2^\circ$, $2\theta = 50.5^\circ$, and $2\theta = 70.4^\circ$, for Cu(111), Cu(200) and Cu(220), respectively, in metallic Cu. In Cu/AC, CuO and Cu₂O, were also detected²⁷. Graphite, C, was present in all catalysts studied except Cu/ZnO, with a constant peak at $2\theta = 26.6^\circ$ that corresponds to C(002)²⁸. In the catalysts with ZnO in their constitution, the crystallite form zincite was identified²⁹.

X-ray photoelectron spectroscopy (XPS)

Five peaks were identified in the C 1s region (Figure S12), corresponding to the aromatic and aliphatic carbon, (C1) at 284.8 eV, phenols, and CN groups (C2) at 286.1 ± 0.1 eV, keto-groups (C3) at 288.0 ± 0.1 eV, carboxylic groups (C4) at 289.6 eV, and the plasmon loss (Cshake-up) at 291.7 ± 0.1 eV^{32,33}.

In the O 1s region (Figure S13), the peak identified at 530.9 ± 0.2 eV (O1) can be attributed to the lattice oxygen of ZnO, the one at 531.8 ± 0.2 eV (O2) can be attributed to oxygen in C=O in CNT, and chemisorbed oxygen caused by the surface hydroxyl groups on ZnO, at 532.6 ± 0.0 eV (O3) is related to hydroxyls, ethers and C=O in esters, amides, and anhydrides in CNT, another at 533.7 ± 0.1 eV (O4), is related to C–O in esters and anhydrides in CNT and finally, the peak at 534.8 eV (O5) is related to carboxylic groups in CNT^{30,32}.

The N 1s spectra (Figure S14) presents mainly pyridinic groups (N1) and pyrrolic (N2) groups at 399 ± 0.1 eV and 400.8 ± 0.1 eV, respectively, as well as some quaternary groups (N3) at 402.5 ± 0.1 eV. It is also possible to observe π excitation at 496 ± 0.1 eV^{19,32}.

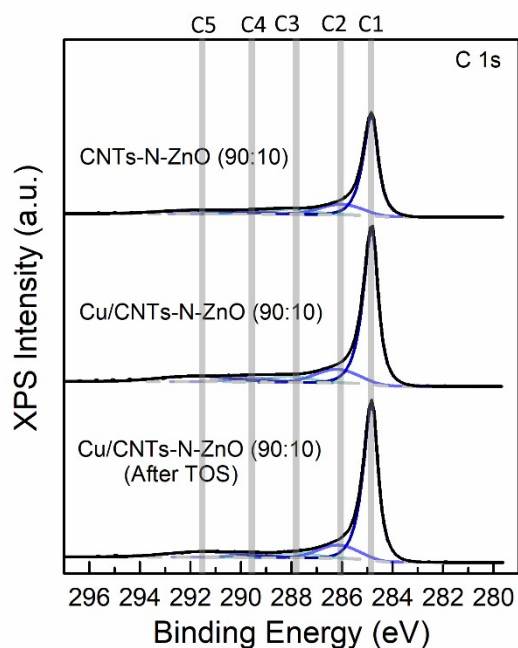


Figure S12. High-resolution XPS data for C 1s for the CNTs-N-ZnO (90:10) support and the fresh and after TOS Cu/CNTs-N-ZnO (90:10). Symbols: raw data; black lines: overall fits; coloured lines: fits of individual components; dashed lines: background. C1: aromatic and aliphatic carbon; C2: phenols, and CN groups; C3: keto groups; C4: carboxylic groups; C5: plasmon loss.

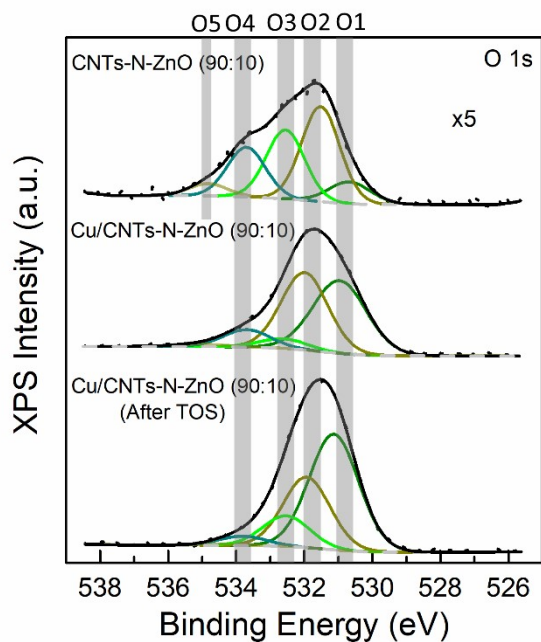


Figure S13. High-resolution XPS data for O 1s for the CNTs-N-ZnO (90:10) support and the fresh and after TOS Cu/CNTs-N-ZnO (90:10). Symbols: raw data; black lines: overall fits; coloured lines: fits of individual components; dashed lines: background. O1: lattice oxygen of ZnO, O2: oxygen in C=O in CNT, and chemisorbed oxygen caused by the surface hydroxyl groups on ZnO, O3: hydroxyls, ethers, and C=O in esters, amides, and anhydrides in CNT, O4: C–O in esters and anhydrides in CNT, O5: carboxylic groups in CNT.

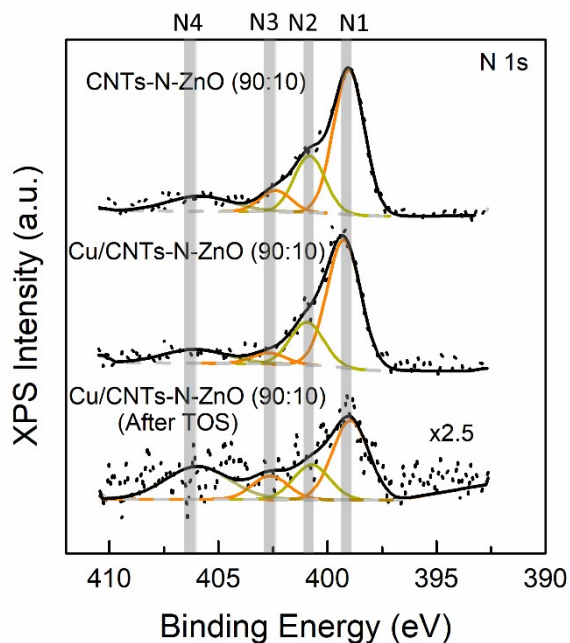


Figure S14. High-resolution XPS data for N 1s for the CNTs-N-ZnO (90:10) support and the fresh and after TOS Cu/CNTs-N-ZnO (90:10). Symbols: raw data; black lines: overall fits; coloured lines: fits of individual components; dashed lines: background. N1: pyridinic groups; N2: pyridonic or pyrrolic groups; N3: quaternary groups; N4: π excitation.

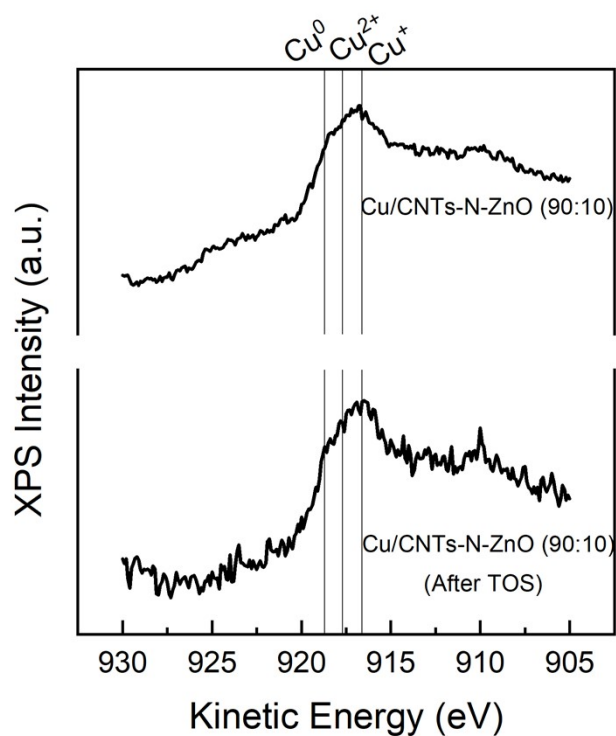


Figure S15. High-resolution XPS data for Cu LMM for the fresh and after TOS Cu/CNTs-N-ZnO (90:10). Symbols: raw data; black lines: overall fits; coloured lines: fits of individual components; dashed lines: background.

Additional Discussion

Table S4. Comparison of the obtained results for the best performing catalyst on the RWGS reaction with other publications.

| <i>Catalyst</i> | <i>Catalyst's mass</i> | <i>P</i> [bar] | <i>T</i> [°C] | <i>H₂:C</i> <i>O₂</i> | <i>WHSV</i> [mL g _{cat} ⁻¹ h ⁻¹] | <i>X_{CO2}</i> [%] | <i>S_{CO}</i> [%] | <i>Reference</i> |
|-------------------------------------|------------------------|-------------------|------------------|--|---|-------------------------------|------------------------------|------------------|
| 10%Cu/SiO ₂ | 0.02 | 1 | 600 | 1 | 120 000 | 8.0 | 100 | 36 |
| 0.3%Fe/SiO ₂ | 0.02 | 1 | 600 | 1 | 120 000 | 2.0 | 100 | 36 |
| 10:0.3 CuFe/SiO ₂ | 0.02 | 1 | 600 | 1 | 120 000 | 12 | 100 | 36 |
| Pd/SiO ₂ | 0.05 | 1 | 600 | 1 | 60 000 | 29 | 82.0 | 37 |
| PdIn/SiO ₂ | 0.05 | 1 | 600 | 1 | 60 000 | 10 | 100 | 37 |
| CuNi/Al ₂ O ₃ | 0.5 | 1 | 600 | 1 | 2 000* | 28.7 | 79.7 | 38 |

| | | | | | | | | |
|-----------------------|-----|---|-----|---|---------|------|-----|--------------|
| 6.5%Cu/ZnO | 0.2 | 1 | 600 | 3 | 9 000 | 42.5 | - | 22 |
| Cu/ZnO | 0.1 | 1 | 600 | 4 | 60 000* | 34.9 | 100 | Present work |
| Cu/CNTs-N-ZnO (90:10) | 0.1 | 1 | 600 | 4 | 60 000* | 54.8 | 100 | Present work |

*Corresponds to GHSV

References

- 19 L. P. L. Gonçalves, J. P. S. Sousa, O. S. G. P. Soares, O. Bondarchuk, O. I. Lebedev, Y. V. Kolen'ko and M. F. R. Pereira, *Catal. Sci. Technol.*, 2020, **10**, 7217.
- 22 J. Wen, C. Huang, Y. Sun, L. Liang, Y. Zhang, Y. Zhang, M. Fu, J. Wu, L. Chen and D. Ye, *Catalysts*, 2020, **10**, 533.
- 23 M. Thommes, K. Kaneko, A. V. Neimark, J. P. Olivier, F. Rodriguez-Reinoso, J. Rouquerol and K. S. W. Sing, *Pure Appl. Chem.*, 2015, **87**, 1051.
- 25 R. Rocha, O. Soares, J. Figueiredo and M. Pereira, *C*, 2016, **2**, 17.
- 26 J. L. Figueiredo, M. F. R. Pereira, M. M. A. Freitas and J. J. M. Órfão, *Carbon N. Y.*, 1999, **37**, 1379.
- 27 H. M. A. Hassan, M. S. Alhumaimess, I. H. Alsohaimi, S. K. Mohamed, O. F. Aldosari, T. S. Alraddadi and A. A. Essawy, *Colloids Surfaces A Physicochem. Eng. Asp.*, 2022, **654**, 130056.
- 28 Q. T. Ain, S. H. Haq, A. Alshammari, M. A. Al-Mutlaq and M. N. Anjum, *Beilstein J. Nanotechnol.*, 2019, **10**, 901.
- 29 A. Khorsand Zak, R. Razali, W. H. Abd Majid and M. Darroudi, *Int. J. Nanomedicine*, 2011, **6**, 1399.
- 30 T. Wang, B. Jin, Z. Jiao, G. Lu, J. Ye and Y. Bi, *J. Mater. Chem. A*, 2014, **2**, 15553.
- 32 J. L. Figueiredo and M. F. R. Pereira, *Catal. Today*, 2010, **150**, 2.
- 33 L. P. L. Gonçalves, D. B. Christensen, M. Meledina, L. M. Salonen, D. Y. Petrovykh, E. Carbó-Argibay, J. P. S. Sousa, O. S. G. P. Soares, M. F. R. Pereira, S. Kegnæs and Y. V. Kolen'Ko, *Catal. Sci. Technol.*, 2020, **10**, 1991.
- 36 C. S. Chen, W. H. Cheng and S. S. Lin, *Appl. Catal. A Gen.*, 2004, **257**, 97.
- 37 J. Ye, Q. Ge and C. J. Liu, *Chem. Eng. Sci.*, 2015, **135**, 193.

